

Understanding the Ligand-Assisted Reprecipitation of CsPbBr₃ Perovskite Nanocrystals via High Throughput Robotic Synthesis Approach

Sheryl L Sanchez, Jonghee Yang*, Mahshid Ahmadi*

Institute for Advanced Materials and Manufacturing, Department of Materials Science and Engineering, The University of Tennessee Knoxville, Knoxville, Tennessee, 37996, United States

*Corresponding authors email: jyang70@utk.edu, mahmadi3@utk.edu

Abstract:

Inorganic cesium lead bromide (CsPbBr₃) perovskite nanocrystals (PNCs) have rendered promising performances in various optoelectronic applications. In contrast to the complex hot-injection synthesis, the ligand-assisted reprecipitation (LARP) method renders a simple route enabling mass-production of high-quality PNCs. However, LARP synthesis is susceptible, and thus, little has been deeply understood about how to control the growth of PNCs and the optical characteristics of the PNCs. Herein, by implementing a high-throughput automated experimental platform, we explore the growth behaviors and colloidal stability of the LARP-synthesized PNCs. Using two distinctive acid-base pairs – oleic acid-oleylamine and octanoic acid-octylamine, we systematically explore the influence of ligands – chain lengths, concentration and ratios – on the particle growths and consequent functionalities of the PNCs. We observe that the short-chain ligands cannot make functional PNCs with desired sizes and shapes, whereas the long-chain ligands provide homogeneous and stable PNCs. The PNCs transform into a Cs-rich non-perovskite structure with poorer emission functionalities and larger size distributions by employing excessive amines or polar antisolvent. This proposes that the diffusion of the ligands in a reaction system crucially determines the structures and functionalities of the PNCs. Our high-throughput exploration provides a detailed guidance on synthesis routes for desired PNCs.

Introduction

Lead halide perovskite nanocrystals (PNCs) are one of the most promising materials for the use in optoelectronic applications including photovoltaics^{1,2} and light-emitting diodes.^{3,4} This is due to their excellent optical characteristics tunable across a wide bandgap range and solution processability. All-inorganic CsPbBr₃ NCs demonstrate narrow emission bands,^{5,6} high photoluminescence quantum yields^{7,8} and great intrinsic stability^{5,9,10} in comparison to the organic metal halide perovskite counterparts, which lack long-term stability under ambient conditions.

Conventionally, the PNCs have been synthesized via hot-injection method by adding the precursor stock in a reaction flask in an elevated temperature and inert atmosphere. The resulting PNCs reproducibly exhibits narrow size distributions and excellent optical characteristics that are directed to device applications. However, the hot-injection method requires a dedicated reaction system and a sequence of multiple step in a synthetic procedure that are complex and energy-inefficient and, essentially not suited for mass-production.

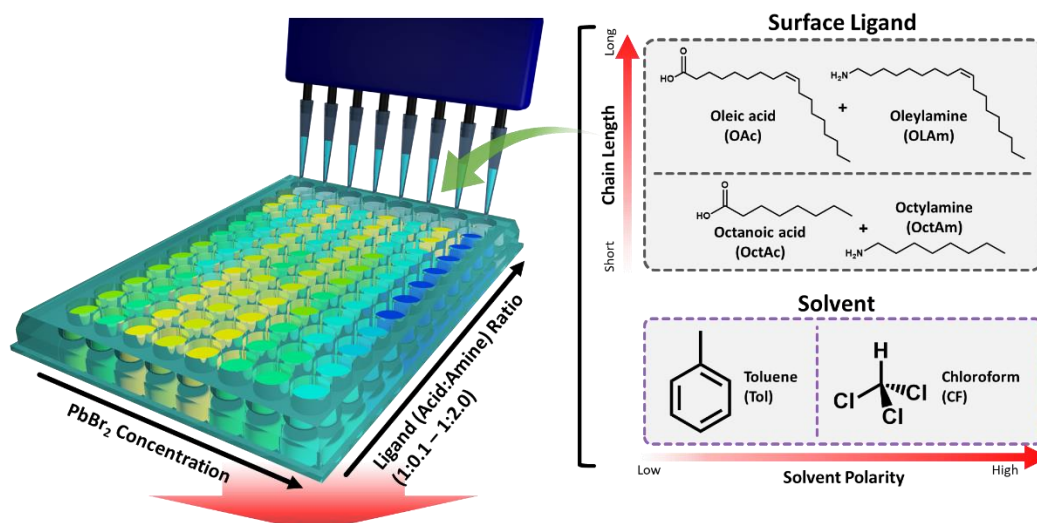
In contrast, ligand-assisted reprecipitation (LARP) method is proposed as a promising alternative in mass-producible PNC synthesis route, which simply synthesizes the PNCs having compatible functionalities.¹¹⁻¹³ Particularly, the simple synthetic procedure without requiring a complex infrastructure enables low-cost upscaling to commercial batches. However, the resulting PNCs are relatively susceptible in several post-processing, somewhat losing the desired functionalities for high-performance device applications. Thus, little has been understood on how the ligand properties, the ratio and solvent properties determine the overall size, shape, and stability of PNCs synthesized by LARP method.

Herein, high throughput screening allows for the variability of the synthesis routes to be explored within a few hours rather than weeks and months optimization. The underlying mechanism behind the size, shape and stability control of the nanocrystals are explored through time-dependent photoluminescence (PL) and absorption spectroscopies. Using two unique acid-base ligand pairs – oleic acid-oleylamine and octanoic acid-octylamine, we systematically studied the influence of ligands – chain lengths, concentration and ratios – on particle growth and subsequent functionalities of PNCs. The desired size and shape of the PNCs were successfully produced by the long-chain ligands providing uniform and stable NCs. The use of excessive amines or polar antisolvents was found to transform the PNCs into Cs-rich non-perovskite structures that exhibit larger size distributions and lower emission functions. These features are an indication that the ionic diffusion of ligands in a reaction system determines the structures and functions of the PNCs crucially. Crucially, these results are also the counterevidence against the common notion that the use of polar solvents for dissolving inorganic precursors (e.g., *N,N*-dimethylformamide (DMF)) is detrimental to PNC stability; *selection of antisolvent can be more critical*. Our high-throughput exploration provides accelerated detailed instructions on the synthesis paths for the desired PNCs.

Discussion

Ligands can influence the optical properties of CsPbBr₃ PNCs by modifying their sizes/shapes that are directed to the resulting surface energy levels and bandgap.¹⁴⁻¹⁷ Each ligand type is utilized due to their unique chemical actions – depending on its molecular structure and reactivity,^{14, 15, 17} which not only influence on the reaction pathway during synthesis but also the colloidal stability of the resulting PNCs.¹⁸ Carboxylic acids and amines are commonly used in the synthesis of nanocrystals to prevent aggregation and control crystallization, respectively.¹⁹⁻²¹ Note that both carboxylic acids and amines are complementary with each other for PNC synthesis; as the mixing of both chemical species results in acid-to-amine proton transfer, transforming them to ionic carboxylate and ammonium forms that are enable to coordinate to the PNC surface.

(a) High-Throughput LARP Synthesis



(b) Automated Characterization and Analysis

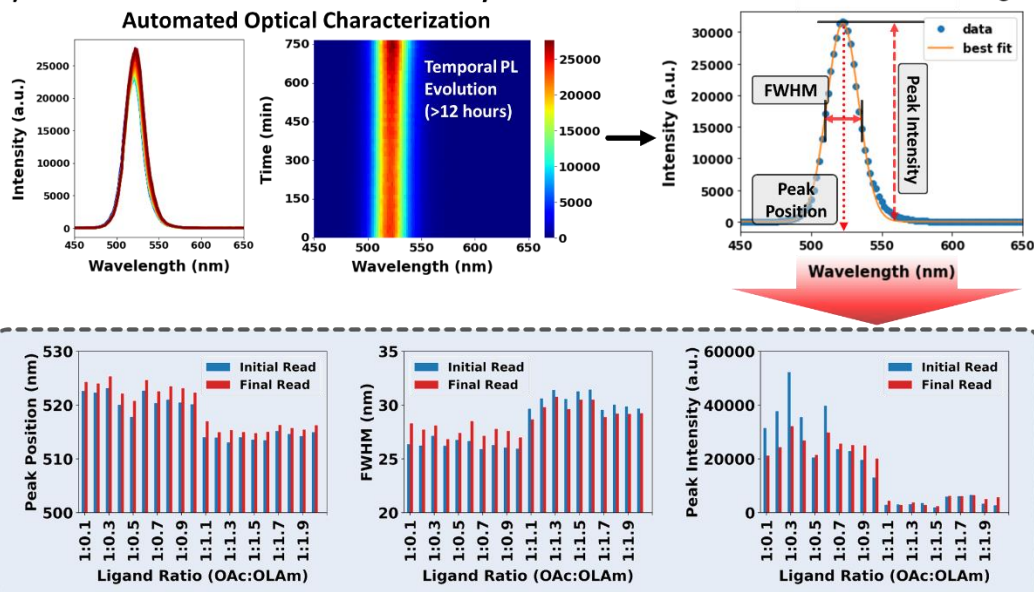


Figure 1: (a) Workflow for the high throughput LARP synthesis of CsPbBr₃ nanocrystals with various ligand ratios, ligand pairs and solvent. (b) Automated characterization and analysis of the synthesized CsPbBr₃ nanocrystals.

High-throughput exploration on the growth behaviors of LARP-synthesized CsPbBr₃ PNCs was performed by utilizing an integrated automated synthesis-characterization system.²² The high-throughput LARP synthesis was performed using the OT-2 pipetting robot (Opentron), by injecting the PbBr₂ solutions (in DMF) with various PbBr₂ concentrations and the ligand ratios into the Cs-containing antisolvent in each well, as shown in **Figure 1a**. Here we devised a modified LARP synthesis protocol to improve the reproducibility of the synthesis (see **Methods, Figure S1 and S2**). Two pairs of surface ligands, oleic acid (OAc) with oleylamine (OLAm) and octanoic acid (OctAc) and octylamine (OctAm) are selected to explore the effect of the length and ratio of the ligand on the resulting PNCs. The precursor solution is then injected into two different antisolvents with different polarities (i.e., toluene and chloroform) to see the effect it may have on the formation of the CsPbBr₃ NCs. A detailed explanation of the high-throughput synthesis workflow can be found in the Supporting Information.

After the synthesis of PNC, the well plate is subsequently transferred into a high-throughput optical reader and the emission properties and colloidal stability of the PNCs are characterized by monitoring photoluminescence (PL) spectra for over 12 hours. The underlying mechanisms within the compositions were then investigated by time-dependent PL, where the change of overall intensity, peak position, and full-width at half maximum (FWHM) are quickly traced through automated gaussian fitting (**Figure 1b**). This overall experimental workflow provides rich data that gives high-throughput insights into the optical properties, stability, and structural changes of the PNCs over time.

LARP synthesis of CsPbBr₃ PNCs are influenced by various factors including phase transitions, ligand-binding and degradation mechanisms. These can occur with variability of the synthesis parameters, all which correspondingly changes the shapes, sizes and size distributions of PNCs and the resulting PL spectra. Typically, the functional CsPbBr₃ NC with a nominal size of ~20 nm can be characterized by having a cubic structure, showing a green PL (peak at ~520 nm in PL spectrum).^{5, 23, 24} The size of PNCs can affect the position of the PL peak wavelength; the larger in PNC size, the shorter PL peak wavelength is expected.

The cubic CsPbBr₃ phase can be transformed to the hexagonal Cs-rich Cs₄PbBr₆, exhibiting insulator characteristics.^{5, 24, 25} The [PbBr₆]⁴⁻ octahedra become disintegrated from the CsPbBr₃ lattice, transforming to the hexagonal Cs-rich phase. The [PbBr₆]⁴⁻ octahedra of Cs₄PbBr₆ are spatially isolated from each other in its lattice structure, thus creating a wide band gap of 3.9 eV.^{5, 24-26} Within the reaction system, the Cs₄PbBr₆ formation in turn consumes both Cs⁺ and [PbBr₆]⁴⁻ building blocks intended to be formed as CsPbBr₃, manifesting translucent solution and suppression of green PL with larger FWHM.^{21, 27, 28} Meanwhile, it is reported that excessive amines – by making Pb-amine complexes – would also induce the phase transformation from CsPbBr₃ to the Cs-rich Cs₄PbBr₆.^{23, 27, 29} Together, the overall workflow proposed in this work based on high-throughput robotic platform allows us to comprehensively understand the LARP synthesis of CsPbBr₃ PNCs, thereby rendering the overall synthesis landscape of the PNCs. Subsequently, this not only revealing the tendencies of structural changes or the thresholds for (undesired) phase

transformations as a function of precursor concentrations and/or ligand ratios, but also suggest an optimal synthetic condition to realize highly-functional PNC ensembles.

As a preliminary study, the proposed workflow is implemented to explore the influence of overall ligand concentration in the precursor solutions before being injected into the Cs-containing antisolvent in a reaction well. Starting with a conventional ligand pair – OAc and OLAm – for the PNC synthesis, two ligand concentrations – 1:15 and 1:30 v/v ratios between the ligand and PbBr_2 solution – are selected (**Figure S3**). The former ratio is comparable with the nominal ligand concentrations typically utilized for the LARP synthesis. From each PL spectrum with a ligand ratio, the resulting PL characteristics (i.e., peak positions, intensities, and FWHMs) at the specific timepoint ($t=0$ and 12 hours) are automatically extracted, as shown in Figure 2. In **Figure 2a and b**, the peak positions of the PNCs are within the similar wavelength range around ~ 515 nm. In fact, it has been reported that both the intact CsPbBr_3 PNCs and Cs_4PbBr_6 NCs where CsPbBr_3 PNCs are residually doped can emit green PL over 500 nm.^{23,24, 30, 31,42,43} Therefore, the emergence of Cs-rich Cs_4PbBr_6 NPs is essentially not distinguishable by sole judgement from the PL peak positions. However, the colorless dispersions in the well plate suggest the phase transformation to Cs_4PbBr_6 NCs (**Figure S2**).

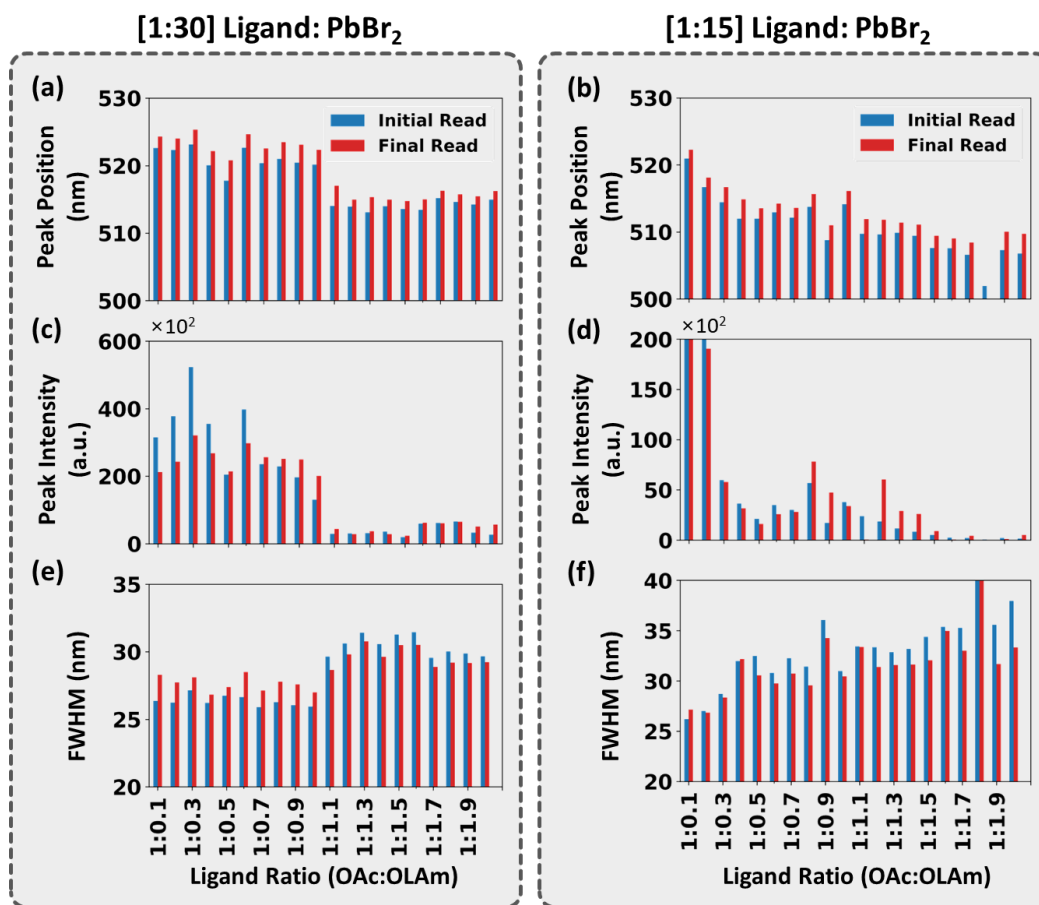


Figure 2: Automatically extracted PL characteristics of CsPbBr_3 PNCs synthesized with OAc:OLAm Ligands in Toluene: (a, b) PL peak positions, (c, d) peak intensities, and (e, f)

FWHMs, respectively. Two different volume ratios of ligand, i.e., OAc:PbBr₂ precursor solution (50 mM in DMF) are used: (a) 1:30 and (b) 1:15.

The major differences in PL characteristics of these NCs are seen in their PL intensities and FWHMs (**Figure 2c-f**). With increasing the concentration of amine in precursors, the significant intensity drops and broadenings in PL peaks – a signature for the formation of Cs-rich NC – is observed; excessive amine can react with Pb ions to form amine-Pb complexes, which cannot contribute to the formation of CsPbBr₃ PNC but result in Cs-rich Cs₄PbBr₆ phase.^{27, 32, 33} Note that the drop in PL intensity and the widening of the FWHM is more apparent with higher ligand concentration (i.e., 1:15, which is actually a nominal ligand concentration for LARP synthesis) for the PNC synthesis.¹¹⁻¹³ Higher concentration of ligands (0.2-0.6 M depending on the added OLAm) than that of PbBr₂ (0.15 M of ions assuming a complete ion dissociation) in the precursor solutions could solvate the inorganic ions much stronger, thereby disintegrating the crystallized inorganic nuclei and/or the prematured PNCs. This might not only increase the chance for the formation of Cs-rich phase rather than CsPbBr₃ but also result in a larger size distribution, respectively mirrored as the lower PL intensities and larger FWHMs. Hereafter, the ligand:PbBr₂ ratio is fixed to 1:30 in this study, which provided better reproducibility and optical characteristics.

At an optimized OAc:OLAm ligand concentration, we see that when OAc is in majority (i.e., OAc > OLAm), the synthesized PNCs exhibit longer PL wavelength >520 nm, as shown in Figure 2(a). they preserve fairly strong PL intensities (**Figure 2c**) and reasonable FWHM value around 26 nm (**Figure 2e**) even after 12 hours. An increase of OLAm blueshifts the PL of the PNCs, which is an indication of a smaller NC. Meanwhile, the peak intensity is suppressed with a larger FWHM values around 30 nm, speculating the emergence of Cs₄PbBr₆ NCs that would be attributed to Pb-amine complexes formation.^{27, 32, 33}

Further, the role of ligand chain length is investigated in our system, where we vary the ligand ratio of the 18 carbon OAc/OLAm and the ratio of the 8 carbon OctAc/OctAm ligands. The chain length variations of the amines and acids was shown to have a correlation with the size and shape of nanocrystals.^{15, 34-36} The extracted PL characteristics of CsPbBr₃ PNCs synthesized with OctAc/OctAm ligands are shown in **Figure S4 and S5**. A sudden blueshift in peak position when the concentration of OctAm exceeds that of OctAc (**Figure S5a**), implying the smaller sizes of NCs are synthesized at these conditions. Mixing of both OctAc and OctAm leads to proton transfer and respectively converts them to octanoate and octylammonium forms, which can participate into the PNC surface coordination. In OctAm-majority conditions, the excessive OctAm molecules cannot be protonated from the acid. Analogous to the observations in OAc/OLAm systems, these Lewis base ligand? could be responsible for the PL blueshifts; they attack the Pb and form the amine-Pb complexes, which prevent the precursor ion to grow the PNC larger.³⁷

The peak intensity exhibits a lack of trend for the OctAc/OctAm ligands (**Figure S5b**), which is an indication the stable PNC formation may not be much favorable in this system; an increase or decrease in peak intensity over time may be due to the gradual PNC growth or complete decomposition of the PNC. As can be seen in **Figure S5c** the FWHM of the NCs are about ~27.5 nm when OctAc is in majority and a slight increase in FWHM ~35 nm is observed when OctAm increases. The weaker van der Waals (vdW) interaction among the shorter-chain ligands and the

consequent smaller surface energy, the smaller ligand-confined reverse micelles (RMs) producing the PNCs with smaller surface-to-volume ratios tend to be formed in the solution.³⁸ Meanwhile, these RMs would be relatively unstable in the polar reaction mixture system, due to the larger portion of polar heads (i.e., carboxylate and ammonium) in the ligands (particularly, the amine-excessive compositions) compared with the longer-chain ligand pairs. Thus, the synthesis of the PNCs is unlikely favorable in OctAc/OctAm system.

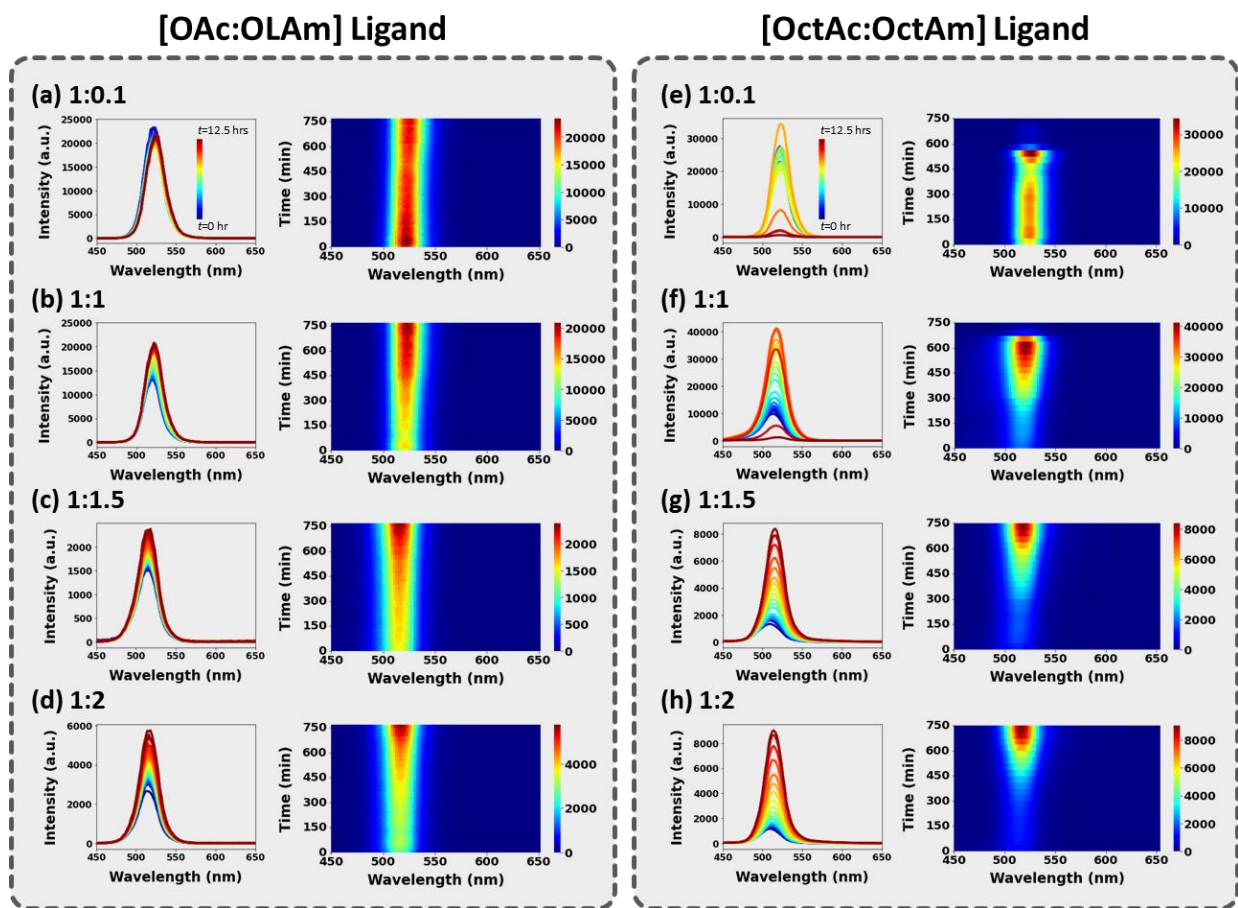


Figure 3: (a-d) Time dependent photoluminescence spectra and corresponding heat maps of CsPbBr_3 PNCs with various ligand ratios of OAc/OLAm in Toluene: (a) 1:0.1, (b) 1:1, (c) 1:1.5 and (d) 1:2, respectively. (e-h) Time dependent photoluminescence spectra and corresponding heat maps of CsPbBr_3 PNCs with various ligand ratios of OctAc/OctAm in Toluene: (a) 1:0.1, (b) 1:1, (c) 1:1.5 and (d) 1:2, respectively.

The discrepancies in temporal PL changes of the PNCs prepared by different ligand pairs and ratios are also visualized in the PL spectra and spectro-temporal maps shown in **Figure 3**. It is immediately apparent that ligand type has an impact on the overall PL evolution; OAc/OLAm exhibits relatively little change in peak intensity and position over time (**Figure 3a-d**), whereas

OctAc/OctAm exhibits vast changes over time expressing instability (**Figure 3e-h**). These observations evidently infer that the ligand chain length not only influences on the dimensionality but also the long-term colloidal stability of the resulting CsPbBr₃ PNCs. Note that, in PNC dispersion, the binding of the carboxylate and ammonium ligands are described as a dynamic equilibrium, where the ligands are simultaneously attached and detached at the PNC surface.²⁷ Given the smaller molecular weight of the OctAc and OctAm, more dynamic adsorption/desorption of the ligands (i.e., faster reaction rates) can be anticipated. In turn, This could crucially compromise the colloidal stability of the PNC dispersions, in accordance with our observations.

In continuation of exploring the role of ligand chain length on the morphology and stability of CsPbBr₃ NCs, transmission electron microscopy (TEM) analysis was conducted, the images of PNCs synthesized with OAc and OLAm are shown in **Figure 4a-d**. In **Figure 4a** the TEM image of NCs with a 1:0.1 ratio of OAc/OLAm are cubic and monodispersed. In **Figure 4b** the nanocrystals exhibit a slight increase in size, yet maintain a state of monodispersity. In **Figure 4c** the ligand ratio is 1:1.5 and the OLAm is at the majority here. We can see the presence of ellipsoidal-spherical NPs with a nominal size >100 nm. These NPs are a combination of cubic and hexagonal nanoparticles together,³⁹ most likely in the transition to the Cs-rich nanocrystals. In **Figure 4d** the ligand ratio of 1:2 OAc/OLAm shows mostly hexagonal, aggregated nanoparticles. In addition, we observe variety of NPs including circular or oblong s NPs. The hexagonal shaped features are likely the Cs-rich Cs₄PbBr₆ NCs.³⁹ The aggregation of these NCs are most likely due to the lack of OAc found in the system. This is because OAc is known to regulate the aggregation of NPs while OLAm is known to control their sizes.¹⁹⁻²¹ It is demonstrated that OLAm is facilitating the decomposition process of CsPbBr₃ into Cs₄PbBr₆.

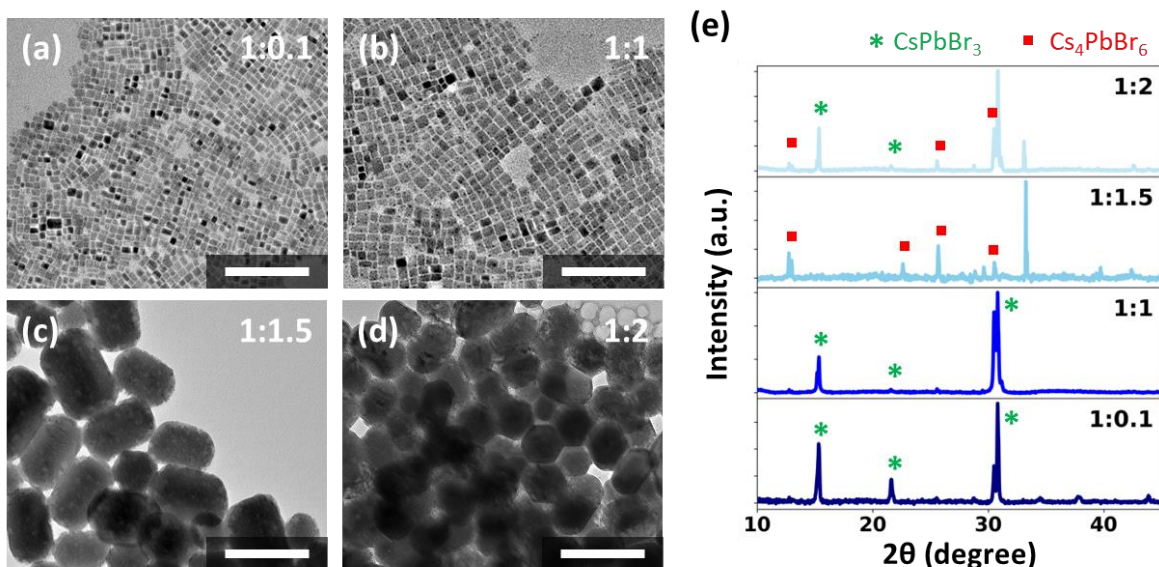


Figure 4: TEM images of CsPbBr₃ PNCs prepared with OAc/OLAm in Toluene with a ratio of (a) 1:0.1, (b) 1:1, (c) 1:1.5 and (d) 1:2, respectively. Scale bar: 200 nm. (e) XRD diffraction patterns

of the corresponding PNCs. Green asterisks and red squares respectively associated with the crystal lattice of CsPbBr_3 and Cs_4PbBr_6 are marked.

TEM images of CsPbBr_3 PNCs synthesized with OctAc/OctAm (at ligand ratio of 1:0.1 and 1:1) were also collected (**Figure S6**). At a 1:0.1 (OctAc/OctAm) ratio, the considerable amounts of PNCs were aggregated or even fused with each other, thereby rendering various sizes as shown in **Figure S6a**. The shorter chained ligands are not effective to produce monodispersed cubic CsPbBr_3 PNCs, analogous to the observations in CsPbI_3 PNCs using a short ligand serving weaker vdW force.¹⁸ Increasing the amine concentration (1:1) shows the coexistence of smaller particles and giant hexagonal-shaped particles as seen in **Figure S6b**. The smaller PNCs can be attributed to the poor binding ability of OctAc/OctAm due to their smaller molecular weight, as speculated in their poor temporal PL stabilities (figure 3e-h).²⁷ The formation of these giant NPs is likely attributed to the formation of Cs-rich Cs_4PbBr_6 NCs,^{33,39} together with the Ostwald ripening.⁴⁰

Corresponding XRD patterns of the CsPbBr_3 PNCs synthesized with OAc/OLAm ligand are shown in **Figure 4e**. We can see that when OAc is in majority, CsPbBr_3 phase is confirmed to be the only phase present. The CsPbBr_3 crystal structure was confirmed to be orthorhombic (*Pnma*) with peak positions at 15.32, 21.59 and 30.81 (2 θ). When the amount of OLAm is increased we observe the co-existence of CsPbBr_3 and Cs_4PbBr_6 phases as indicated in the XRD pattern. The lower dimensional phase agrees with suppression of PL intensity, blue shift and the widening of the FWHM due to insulator-like effect of Cs_4PbBr_6 .^{27,32,33} The XRD results also agree with the TEM images that exhibit CsPbBr_3 nanocrystals when OAc is in majority.^{32,41,42} Here, the trend between ligand ratio has become abundantly clear, so investigation of other parameters effecting the nanocrystals is important in understanding all the changes that can occur.

We attempted to trace the ionic form of PbBr_2 in precursor solution with the ligands. However, the absorption range of the PbBr_2 -based ionic complexes is out of the detection range (**Figure S7**). Alternatively, we monitored the absorption spectra of the PbI_2 ionic complexes in solution as a function of OAc/OAm ratio (**Figure S8**). We observe two distinctive peaks at 280 and 320 nm upon addition of pure OAc, respectively assigned to be positive-charged $[\text{PbI}]^+$ and charge-neutral $[\text{PbI}_2]$ complexes.^{43,44} With increasing OLAm molar ratios, the $[\text{PbI}_2]$ peak reduced and disappeared, suggesting that polar $[\text{PbI}]^+$ species are dominant in the precursor system by increasing OLAm molar ratio. This could cause the faster diffusion of the precursors in a reaction system and the PNC formation more dynamic⁴⁵, resulting in poorer PNCs with broader size distributions as seen from the OctAc/OctAm cases.

Interaction of ligand with solvent is not only crucial for the colloidal stability of the PNCs, but also a determinant factor in their synthesis; it can influence on the optoelectronic properties and phase developments of the resulting PNCs. Recall the ionic nature of the PNC lattice bonding and therefore, the polar and ionic heads (i.e., carboxylates and ammoniums) are required for ligand surface coordination. Polar solvents can strongly interact with such ionic ligands (i.e., attraction), thus leading to their solvation – a competitive process with ligand binding onto the PNC surface – more feasible at the end.¹⁸ As a consequence, the more polar solvent rendering stronger ligand-solvent interaction is used, the more likely the nanocrystal lose the colloidal and structural integrity; indeed, faster diffusion of OAc in CDCl_3 compared to Tol-*d*₈ was evidenced by diffusion

ordered nuclear magnetic resonance spectroscopy.⁴⁶ This subsequently leads to different morphologies and crystal phases over time. In light of this, next the effect of solvent on the PNC synthesis is evaluated. We explore the PL characteristics of CsPbBr₃ PNCs synthesized in chloroform— more polar than toluene – as a solvent, as seen in **Figure 5**. Although both are considered a nonpolar solvent, chloroform is more polar than toluene as known by their different dielectric constants and polarity index (2.38 and 2.4 for toluene, and 4.81 and 4.1 for chloroform, respectively).^{47,48}

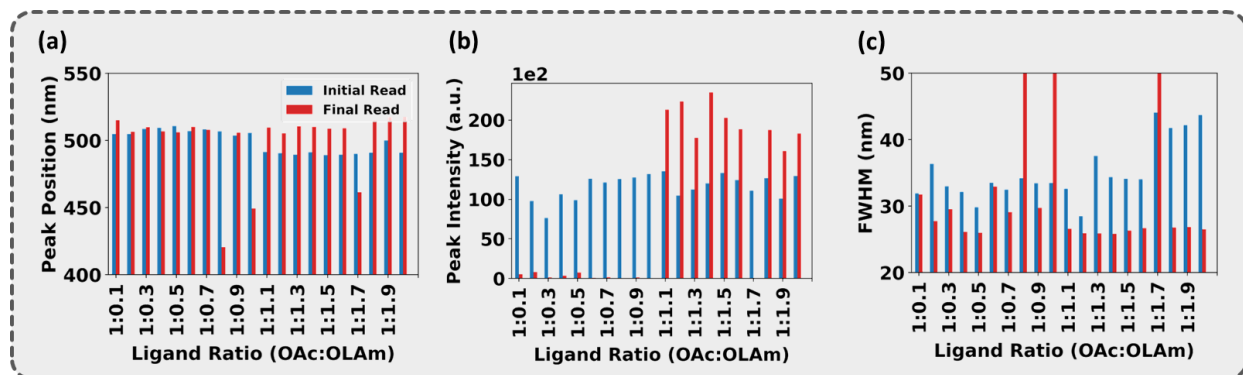


Figure 5: Automatically extracted PL characteristics of CsPbBr₃ PNCs synthesized with OAc/OLAm Ligands (1:30 v/v% vs. PbBr₂ solution) in chloroform: (a) PL peak positions, (b) peak intensities, and (c) FWHMs, respectively.

The role of ligand ratio paired with different polarity of solvents and its effect on the stability of the PNCs is also investigated by monitoring PL evolutions (**Figure S9**). In **Figure 5a**, the PL peak positions exhibit at shorter wavelengths (around 500 nm) than those from toluene (around 520 nm) and undergo blueshifts with increasing OLAm. The PNCs exhibit nominal PL intensities at initial stage, but show different tendencies respectively depending on OAc- or OLAm-majority in ligand compositions after 12 hours (**Figure 5b**). In OAc-majorities, the PL intensities are largely suppressed, whereas notable increases are observed in OLAm-majorities. Meanwhile, there are a broadening tendency in FWHM with increasing the OLAm at the initial stage, but no appreciable differences particularly after 12 hours (**Figure 5c**). In OctAc/OctAm system, the PL peaks initially emerged but they rapidly disappeared, thereby showing no characteristic tendencies in PL properties (**Figure S4 and S10**). This indicates extremely poor colloidal stability of the resulting PNCs in CF environment.

The ligands in former cases (i.e., OAc-majorities) are present in ionic forms, which are prone to be influenced by polar solvent. The enhanced strength in ligand-solvent interaction can shift the equilibrium of ligand binding at the PNC surface towards detachments, gradually causing the PNC decomposition; the fragmented PNC features in TEM image (**Figure S11a**) corroborate this. As a consequence, the emission features of the PNCs become greatly suppressed. Though the PL intensities were increased in OLAm-majority regime, we observe the giant hexagonal-shaped NPs even at the 1:1 ligand ratio (**Figure S11b**) by its decomposition. This suggest that, rather than forming an ensemble where the CsPbBr₃ PNCs are dominant, formation of Cs₄PbBr₆ NC is favored

due to the unprotonated amines as seen in **Figure 4**. Given the strong PL intensity and the moderate FWHMs ~ 25 nm, a plausible scenario to describe the feature is the integration of small CsPbBr₃ PNCs with the Cs₄PbBr₆ NCs during the gradual reaction for 12 hours as previously observed.^{13,39-43}

From our observation, a generalized chemical reaction associated with LARP process, as a function of the carboxylic acid/amine ligand ratio, can be described with infinitesimal RM models that are formed in a reaction system, as proposed in **Figure 6a**. Upon injection of the precursor solution (DMF phase), intuitively the instant formation of ligand RMs at the infinitesimal DMF/solvent (Tol or CF) interface can be envisaged, where the ligand heads confine the inorganic PbBr₂ – both in neutral [PbBr₂] and ionic [PbBr₃]⁻ / [PbBr]⁺ forms – inside the RM. Then, the Cs-oleates dissolved in the solvent phase introduces into the RMs, initiating the crystallization of CsPbBr₃ lattice. The ligands at the RM interface can subsequently coordinate to the lattice surface, thereby producing a dimensionally-confined colloidal PNCs.

The carboxylic acids are used to prevent coagulation of the nanoparticles due to their steric repulsion¹⁵ and decrease halogen vacancies that can be found on the surface of the CsPbBr₃ PNCs.⁴⁹ While the amines are used to control the crystallization, thus controlling the size of the nanocrystals.^{36, 50} At the carboxylic acid-rich regime (i.e., acid>amine), the smaller amounts of ligands could render a smaller RM size, producing smaller PNCs. With increasing the amines, primarily based on the increased amounts of the ligands in the system, larger RMs can be formed which results in the larger PNCs. Note that the increase of amine also results in the increase of the ionic PbBr₂ species, as seen from absorption spectra of the precursor solutions (**Figure S7 and S8**). These ionic forms accelerate the CsPbBr₃ crystallization,⁴⁴ which can result in PNCs with larger defect densities; this is likely responsible for the decrease of PL intensity observed from the PNCs with the OAc:OLAm ratio of 1:0.5~1:1 (**Figure 1**).

At the amine-rich regime, the Pb-amine complex formation is expected.^{37,43} This not only compromises the number of active Pb²⁺ to make CsPbBr₃, but also releases free Br anions. Subsequently, a Cs⁺ and Br⁻-rich condition is manifested, promoting the formation of Cs-rich Cs₄PbBr₆ NCs, rather than the originally intended CsPbBr₃ PNCs. Note that the reactivity of amine is larger for OctAm than OLAm given its dipole moment (**Figure S12**) estimated from *ab initio* calculations, rationalizing the promoted formation of the giant of Cs₄PbBr₆ NCs observed at 1:1 OctAc:OctAm ratio (**Figure S11b**).

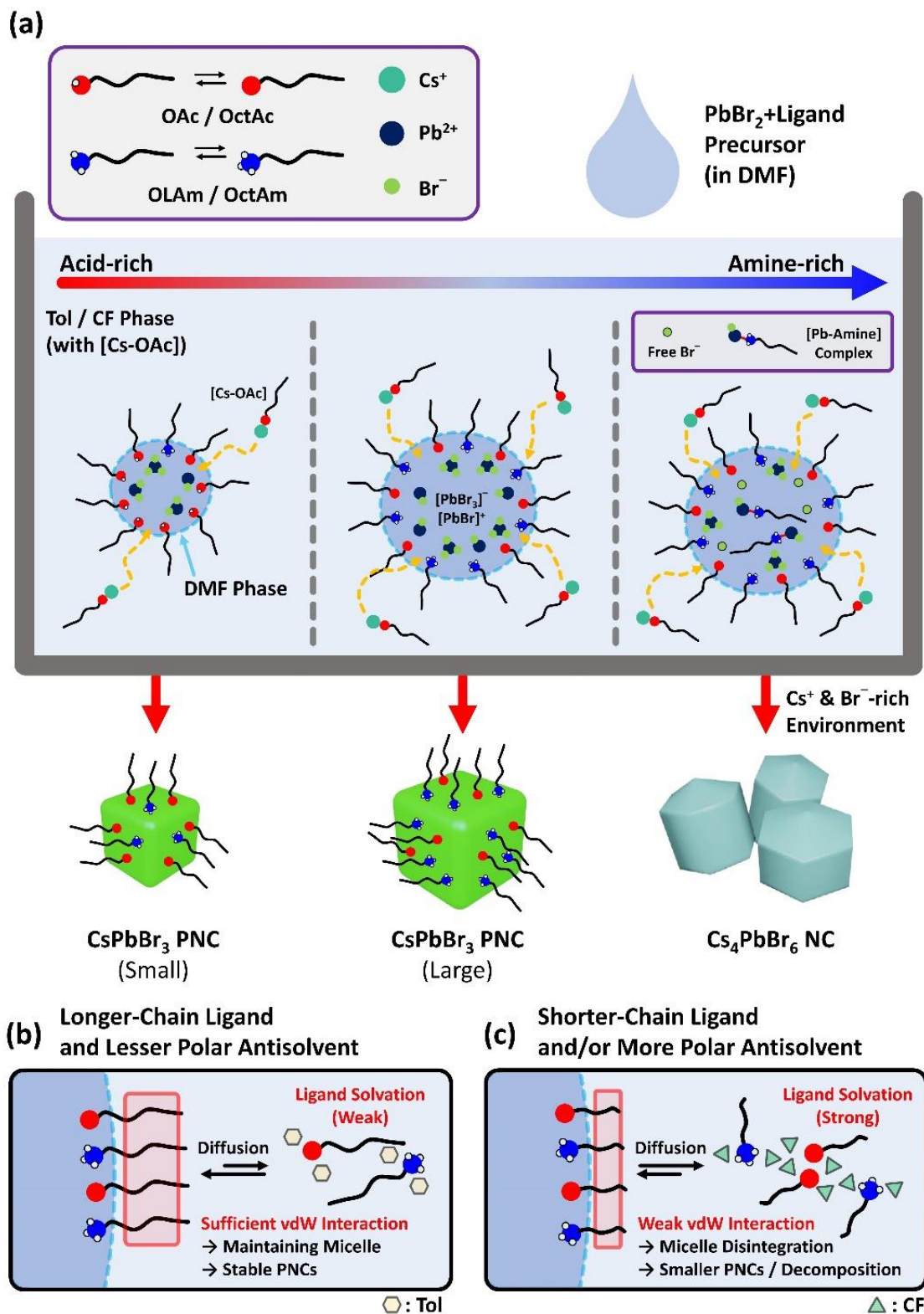


Figure 6. (a) Schematic describing reverse micelle (RM) formation behaviors during LARP process as a function of ligand ratio, which determines the final PNC structures. Schematic

scenarios describing ligand behaviors at RM interfaces: (b) Long-chain ligand and lesser polar antisolvent (OAc/OLAm - toluene), and (c) short-chain ligand and more polar antisolvent (OctAc/OctAm - chloroform)

The vdW interaction of ligand plays a crucial role in PNC synthesis. Larger ligands with a longer alkyl chain provides stronger vdW interaction (i.e., inter-chain attraction) with each other.³⁸ This renders a more rigid RM interface for desired PNC growths, where the ligand solvation and the consequent disassembly of RM is largely mediated under a weakly polar solvent system. In contrast, the use of shorter chain ligands or polar solvents could significantly compromise the rigidity of the RMs and release the ligands to be solvated.^{18,46} As a consequence, poor-shaped PNCs can be obtained.

Through a detailed examination of the PL variability, TEM, and XRD of the synthesized PNCs, we have described the formation behaviors as a function of ligand ratio in **Figure 6a**. The gradual increase of amine in the system leads to the growth of CsPbBr₃ PNCs, eventually leading to a phase transition into Cs-rich NCs. Additionally, we have determined that the chain length and polarity of the antisolvent influence the functionality and structure of the PNCs, as the ionic diffusion of the ligands plays a vital role in the formation of PNCs (**Figure 6b**). It is worth to note that the optimally synthesized PNCs (i.e., 1:0.1 OAc/OLAm) maintained the original PL features over 12 hrs without any purification process, despite the use DMF as a precursor solvent – known to be deleterious for PNC stability. This infers that, counterintuitively, the physicochemical nature of antisolvent is more crucially determines the PNC stability.

Overall, our results highlight the critical role of ligand properties, ligand ratio, and antisolvent properties in the synthesis of PNCs using the LARP method. The high-throughput PL exploration propose an effective way to formulate the PNC formation dynamics in the parametric spaces, which are tightly entangled with each other. Note that state-of-the-art synthesis routes for high-quality PNCs are devised via judicious ligand selections.^{45, 51} Together with these insights, the workflow demonstrated in this study is a powerful tool to construct a detailed chemical map of PNC synthesis, for bespoke tailoring their functionalities.

Conclusion:

In this study, we have executed a high-throughput automated synthesis platform to accelerate the investigation of growth and stability of LARP-synthesized PNCs under various conditions. By using two different acid-base pairs - OAc/OLAm and OctAc/OctAm - we conducted a systematic analysis of the impact of ligand properties, such as chain length, concentration, and ratio, on the growth and functionality of the CsPbBr₃ NCs. Our findings revealed that the use of short-chain ligands (i.e. OctAc/OctAm) and/or polar antisolvent (i.e. CF) result in the production of non-functional PNCs with poor size, shape, and stability. On the other hand, the incorporation of longer-chain ligands produces stable and homogeneous PNCs. However, the use of excessive amines led to the formation of a Cs-rich non-perovskite structure characterized by larger size

distributions and impaired emission functionality. This suggests that the ionic diffusion of the ligands within the system plays a critical role in determining the structure and functionality of the PNCs. Our high-throughput approach provides a firsthand detailed guide for the synthesis of desired PNCs using the LARP method.

Acknowledgment:

All authors acknowledge support from National Science Foundation (NSF), Award Number No. 2043205 and Alfred P. Sloan Foundation, award No. FG-2022-18275. S.S. is partially supported by the UTK-ORNL science alliance program. XRD and TEM were performed at the UTK-Institute for Advanced Materials & Manufacturing (IAMM) Diffraction Facility and Center for Microscopy.

References

- (1) Gratzel, M. The light and shade of perovskite solar cells. *Nat Mater* **2014**, *13* (9), 838-842. DOI: 10.1038/nmat4065 From NLM PubMed-not-MEDLINE.
- (2) Hoffman, J. B.; Zaiats, G.; Wappes, I.; Kamat, P. V. CsPbBr₃ Solar Cells: Controlled Film Growth through Layer-by-Layer Quantum Dot Deposition. *Chemistry of Materials* **2017**, *29* (22), 9767-9774. DOI: 10.1021/acs.chemmater.7b03751.
- (3) Li, C.; Zang, Z.; Chen, W.; Hu, Z.; Tang, X.; Hu, W.; Sun, K.; Liu, X.; Chen, W. Highly pure green light emission of perovskite CsPbBr₃ quantum dots and their application for green light-emitting diodes. *Opt Express* **2016**, *24* (13), 15071-15078. DOI: 10.1364/OE.24.015071 From NLM PubMed-not-MEDLINE.
- (4) Du, X.; Wu, G.; Cheng, J.; Dang, H.; Ma, K.; Zhang, Y.-W.; Tan, P.-F.; Chen, S. High-quality CsPbBr₃ perovskite nanocrystals for quantum dot light-emitting diodes. *RSC Advances* **2017**, *7* (17), 10391-10396. DOI: 10.1039/c6ra27665b.
- (5) Shamsi, J.; Urban, A. S.; Imran, M.; De Trizio, L.; Manna, L. Metal Halide Perovskite Nanocrystals: Synthesis, Post-Synthesis Modifications, and Their Optical Properties. *Chem Rev* **2019**, *119* (5), 3296-3348. DOI: 10.1021/acs.chemrev.8b00644 From NLM PubMed-not-MEDLINE.
- (6) Abir, S. S. H.; Gupta, S. K.; Ibrahim, A.; Srivastava, B. B.; Lozano, K. Tunable CsPb(Br/Cl)₃ perovskite nanocrystals and further advancement in designing light emitting fiber membranes. *Materials Advances* **2021**, *2* (8), 2700-2710. DOI: 10.1039/d1ma00183c.
- (7) Krieg, F.; Ochsenbein, S. T.; Yakunin, S.; Ten Brinck, S.; Aellen, P.; Suess, A.; Clerc, B.; Guggisberg, D.; Nazarenko, O.; Shynkarenko, Y.; et al. Colloidal CsPbX₃ (X = Cl, Br, I) Nanocrystals 2.0: Zwitterionic Capping Ligands for Improved Durability and Stability. *ACS Energy Lett* **2018**, *3* (3), 641-646. DOI: 10.1021/acsenerylett.8b00035 From NLM PubMed-not-MEDLINE.
- (8) Zu, Y.; Dai, J.; Li, L.; Yuan, F.; Chen, X.; Feng, Z.; Li, K.; Song, X.; Yun, F.; Yu, Y.; et al. Ultra-stable CsPbBr₃ nanocrystals with near-unity photoluminescence quantum yield via postsynthetic surface engineering. *Journal of Materials Chemistry A* **2019**, *7* (45), 26116-26122. DOI: 10.1039/c9ta08421e.
- (9) Nenon, D. P.; Pressler, K.; Kang, J.; Koscher, B. A.; Olshansky, J. H.; Osowiecki, W. T.; Koc, M. A.; Wang, L. W.; Alivisatos, A. P. Design Principles for Trap-Free CsPbX₃ Nanocrystals: Enumerating and

- Eliminating Surface Halide Vacancies with Softer Lewis Bases. *J Am Chem Soc* **2018**, *140* (50), 17760-17772. DOI: 10.1021/jacs.8b11035 From NLM PubMed-not-MEDLINE.
- (10) ten Brinck, S.; Zaccaria, F.; Infante, I. Defects in Lead Halide Perovskite Nanocrystals: Analogies and (Many) Differences with the Bulk. *ACS Energy Letters* **2019**, *4* (11), 2739-2747. DOI: 10.1021/acsenergylett.9b01945.
- (11) Brown, A. A. M.; Damodaran, B.; Jiang, L.; Tey, J. N.; Pu, S. H.; Mathews, N.; Mhaisalkar, S. G. Lead Halide Perovskite Nanocrystals: Room Temperature Syntheses toward Commercial Viability. *Advanced Energy Materials* **2020**, *10* (34), 2001349. DOI: <https://doi.org/10.1002/aenm.202001349>.
- (12) Sun, S.; Yuan, D.; Xu, Y.; Wang, A.; Deng, Z. Ligand-Mediated Synthesis of Shape-Controlled Cesium Lead Halide Perovskite Nanocrystals via Reprecipitation Process at Room Temperature. *ACS Nano* **2016**, *10* (3), 3648-3657. DOI: 10.1021/acsnano.5b08193 From NLM PubMed-not-MEDLINE.
- (13) Huang, H.; Raith, J.; Kershaw, S. V.; Kalytchuk, S.; Tomanec, O.; Jing, L.; Susa, A. S.; Zboril, R.; Rogach, A. L. Growth mechanism of strongly emitting CH₃NH₃PbBr₃ perovskite nanocrystals with a tunable bandgap. *Nature Communications* **2017**, *8* (1), 996. DOI: 10.1038/s41467-017-00929-2.
- (14) Kazes, M.; Udayabhaskararao, T.; Dey, S.; Oron, D. Effect of Surface Ligands in Perovskite Nanocrystals: Extending in and Reaching out. *Acc Chem Res* **2021**, *54* (6), 1409-1418. DOI: 10.1021/acs.accounts.0c00712 From NLM PubMed-not-MEDLINE.
- (15) Pan, A.; He, B.; Fan, X.; Liu, Z.; Urban, J. J.; Alivisatos, A. P.; He, L.; Liu, Y. Insight into the Ligand-Mediated Synthesis of Colloidal CsPbBr₃ Perovskite Nanocrystals: The Role of Organic Acid, Base, and Cesium Precursors. *ACS Nano* **2016**, *10* (8), 7943-7954. DOI: 10.1021/acsnano.6b03863.
- (16) Yin, J.; Yang, H.; Gutierrez-Arzaluz, L.; Zhou, Y.; Bredas, J. L.; Bakr, O. M.; Mohammed, O. F. Luminescence and Stability Enhancement of Inorganic Perovskite Nanocrystals via Selective Surface Ligand Binding. *ACS Nano* **2021**, *15* (11), 17998-18005. DOI: 10.1021/acsnano.1c06480 From NLM PubMed-not-MEDLINE.
- (17) Quarta, D.; Imran, M.; Capodilupo, A. L.; Petralanda, U.; van Beek, B.; De Angelis, F.; Manna, L.; Infante, I.; De Trizio, L.; Giansante, C. Stable Ligand Coordination at the Surface of Colloidal CsPbBr₃ Nanocrystals. *J Phys Chem Lett* **2019**, *10* (13), 3715-3726. DOI: 10.1021/acs.jpcclett.9b01634.
- (18) Song, H.; Yang, J.; Jeong, W. H.; Lee, J.; Lee, T. H.; Yoon, J. W.; Lee, H.; Ramadan, A. J.; Oliver, R. D. J.; Cho, S. C.; et al. A Universal Perovskite Nanocrystal Ink for High-Performance Optoelectronic Devices. *Advanced Materials* *n/a* (n/a), 2209486. DOI: <https://doi.org/10.1002/adma.202209486>.
- (19) Imran, M.; Ijaz, P.; Baranov, D.; Goldoni, L.; Petralanda, U.; Akkerman, Q.; Abdelhady, A. L.; Prato, M.; Bianchini, P.; Infante, I.; et al. Shape-Pure, Nearly Monodispersed CsPbBr₃ Nanocubes Prepared Using Secondary Aliphatic Amines. *Nano Lett* **2018**, *18* (12), 7822-7831. DOI: 10.1021/acs.nanolett.8b03598 From NLM PubMed-not-MEDLINE.
- (20) De Roo, J.; Ibáñez, M.; Geiregat, P.; Nedelcu, G.; Walravens, W.; Maes, J.; Martins, J. C.; Van Driessche, I.; Kovalenko, M. V.; Hens, Z. Highly Dynamic Ligand Binding and Light Absorption Coefficient of Cesium Lead Bromide Perovskite Nanocrystals. *ACS Nano* **2016**, *10* (2), 2071-2081. DOI: 10.1021/acsnano.5b06295.
- (21) Ravi, V. K.; Santra, P. K.; Joshi, N.; Chugh, J.; Singh, S. K.; Rensmo, H.; Ghosh, P.; Nag, A. Origin of the Substitution Mechanism for the Binding of Organic Ligands on the Surface of CsPbBr₃ Perovskite Nanocubes. *The Journal of Physical Chemistry Letters* **2017**, *8* (20), 4988-4994. DOI: 10.1021/acs.jpcclett.7b02192.
- (22) Heimbrook, A.; Higgins, K.; Kalinin, S. V.; Ahmadi, M. Exploring the physics of cesium lead halide perovskite quantum dots via Bayesian inference of the photoluminescence spectra in automated experiment. *Nanophotonics* **2020**, *10* (8), 1977-1989. DOI: doi:10.1515/nanoph-2020-0662 (accessed 2022-12-20).
- (23) Akkerman, Q. A.; Park, S.; Radicchi, E.; Nunzi, F.; Mosconi, E.; De Angelis, F.; Brescia, R.; Rastogi, P.; Prato, M.; Manna, L. Nearly Monodisperse Insulator Cs₄PbX₆ (X = Cl, Br, I) Nanocrystals, Their Mixed

- Halide Compositions, and Their Transformation into CsPbX₃ Nanocrystals. *Nano Lett* **2017**, *17* (3), 1924-1930. DOI: 10.1021/acs.nanolett.6b05262 From NLM PubMed-not-MEDLINE.
- (24) Saidaminov, M. I.; Almutlaq, J.; Sarmah, S.; Dursun, I.; Zhumeckenov, A. A.; Begum, R.; Pan, J.; Cho, N.; Mohammed, O. F.; Bakr, O. M. Pure Cs₄PbBr₆: Highly Luminescent Zero-Dimensional Perovskite Solids. *ACS Energy Letters* **2016**, *1* (4), 840-845. DOI: 10.1021/acsenergylett.6b00396.
- (25) Zou, S.; Liu, C.; Li, R.; Jiang, F.; Chen, X.; Liu, Y.; Hong, M. From Nonluminescent to Blue-Emitting Cs₄PbBr₆ Nanocrystals: Tailoring the Insulator Bandgap of 0D Perovskite through Sn Cation Doping. *Advanced Materials* **2019**, *31* (24), 1900606. DOI: <https://doi.org/10.1002/adma.201900606>.
- (26) S Kondo, K. A. a. T. S. localized optical absorption in Cs₄PbBr₆. *Journal of Physics Condensed Matter* **2002**, *14*.
- (27) Li, Y.; Huang, H.; Xiong, Y.; Kershaw, S. V.; Rogach, A. L. Reversible transformation between CsPbBr₃ and Cs₄PbBr₆ nanocrystals. *CrystEngComm* **2018**, *20* (34), 4900-4904, 10.1039/C8CE00911B. DOI: 10.1039/C8CE00911B.
- (28) Wu, L.; Hu, H.; Xu, Y.; Jiang, S.; Chen, M.; Zhong, Q.; Yang, D.; Liu, Q.; Zhao, Y.; Sun, B.; et al. From Nonluminescent Cs₄PbX₆ (X = Cl, Br, I) Nanocrystals to Highly Luminescent CsPbX₃ Nanocrystals: Water-Triggered Transformation through a CsX-Stripping Mechanism. *Nano Lett* **2017**, *17* (9), 5799-5804. DOI: 10.1021/acs.nanolett.7b02896 From NLM PubMed-not-MEDLINE.
- (29) Palazon, F.; Almeida, G.; Akkerman, Q. A.; De Trizio, L.; Dang, Z.; Prato, M.; Manna, L. Changing the Dimensionality of Cesium Lead Bromide Nanocrystals by Reversible Postsynthesis Transformations with Amines. *Chem Mater* **2017**, *29* (10), 4167-4171. DOI: 10.1021/acs.chemmater.7b00895 From NLM.
- (30) Guan, M.; Li, P.; Wu, Y.; Liu, X.; Xu, S.; Zhang, J. Highly efficient green emission Cs₄PbBr₆ quantum dots with stable water endurance. *Opt Lett* **2022**, *47* (19), 5020-5023. DOI: 10.1364/OL.471088 From NLM PubMed-not-MEDLINE.
- (31) Cha, J. H.; Han, J. H.; Yin, W.; Park, C.; Park, Y.; Ahn, T. K.; Cho, J. H.; Jung, D. Y. Photoresponse of CsPbBr₃ and Cs₄PbBr₆ Perovskite Single Crystals. *J Phys Chem Lett* **2017**, *8* (3), 565-570. DOI: 10.1021/acs.jpcclett.6b02763 From NLM PubMed-not-MEDLINE.
- (32) Liu, Z.; Bekenstein, Y.; Ye, X.; Nguyen, S. C.; Swabeck, J.; Zhang, D.; Lee, S. T.; Yang, P.; Ma, W.; Alivisatos, A. P. Ligand Mediated Transformation of Cesium Lead Bromide Perovskite Nanocrystals to Lead Depleted Cs₄(PbBr₆) Nanocrystals. *J Am Chem Soc* **2017**, *139* (15), 5309-5312. DOI: 10.1021/jacs.7b01409 From NLM PubMed-not-MEDLINE.
- (33) Ma, Z.; Li, F.; Zhao, D.; Xiao, G.; Zou, B. Whether or Not Emission of Cs₄PbBr₆ Nanocrystals: High-Pressure Experimental Evidence. *CCS Chemistry* **2020**, *2* (2), 71-80. DOI: 10.31635/ccschem.020.201900086.
- (34) Imran, M.; Di Stasio, F.; Dang, Z.; Canale, C.; Khan, A. H.; Shamsi, J.; Brescia, R.; Prato, M.; Manna, L. Colloidal Synthesis of Strongly Fluorescent CsPbBr₃ Nanowires with Width Tunable down to the Quantum Confinement Regime. *Chem Mater* **2016**, *28* (18), 6450-6454. DOI: 10.1021/acs.chemmater.6b03081 From NLM PubMed-not-MEDLINE.
- (35) Yuan, Y.; Liu, Z.; Liu, Z.; Peng, L.; Li, Y.; Tang, A. Photoluminescence and self-assembly of cesium lead halide perovskite nanocrystals: Effects of chain length of organic amines and reaction temperature. *Applied Surface Science* **2017**, *405*, 280-288. DOI: <https://doi.org/10.1016/j.apsusc.2017.02.024>.
- (36) Almeida, G.; Goldoni, L.; Akkerman, Q.; Dang, Z.; Khan, A. H.; Marras, S.; Moreels, I.; Manna, L. Role of Acid-Base Equilibria in the Size, Shape, and Phase Control of Cesium Lead Bromide Nanocrystals. *ACS Nano* **2018**, *12* (2), 1704-1711. DOI: 10.1021/acsnano.7b08357.
- (37) Kerner, R. A.; Schloemer, T. H.; Schulz, P.; Berry, J. J.; Schwartz, J.; Sellinger, A.; Rand, B. P. Amine additive reactions induced by the soft Lewis acidity of Pb²⁺ in halide perovskites. Part I: evidence for Pb-alkylamide formation. *Journal of Materials Chemistry C* **2019**, *7* (18), 5251-5259, 10.1039/C8TC04871A. DOI: 10.1039/C8TC04871A.

- (38) Aharon, S.; Wierzbowska, M.; Etgar, L. The Effect of the Alkylammonium Ligand's Length on Organic–Inorganic Perovskite Nanoparticles. *ACS Energy Letters* **2018**, *3* (6), 1387-1393. DOI: 10.1021/acseenergylett.8b00554.
- (39) Weerd, C.; Lin, J.; Gomez, L.; Fujiwara, Y.; Suenaga, K.; Gregorkiewicz, T. Hybridization of Single Nanocrystals of Cs₄PbBr₆ and CsPbBr₃. *J Phys Chem C Nanomater Interfaces* **2017**, *121* (35), 19490-19496. DOI: 10.1021/acs.jpcc.7b05752 From NLM PubMed-not-MEDLINE.
- (40) Koolyk, M.; Amgar, D.; Aharon, S.; Etgar, L. Kinetics of cesium lead halide perovskite nanoparticle growth; focusing and de-focusing of size distribution. *Nanoscale* **2016**, *8* (12), 6403-6409. DOI: 10.1039/c5nr09127f From NLM PubMed-not-MEDLINE.
- (41) Wang, L.; Liu, H.; Zhang, Y.; Mohammed, O. F. Photoluminescence Origin of Zero-Dimensional Cs₄PbBr₆ Perovskite. *ACS Energy Letters* **2019**, *5* (1), 87-99. DOI: 10.1021/acseenergylett.9b02275.
- (42) Li, M.; Zhang, X.; Dong, T.; Wang, P.; Matras-Postolek, K.; Yang, P. Evolution of Morphology, Phase Composition, and Photoluminescence of Cesium Lead Bromine Nanocrystals with Temperature and Precursors. *The Journal of Physical Chemistry C* **2018**, *122* (50), 28968-28976. DOI: 10.1021/acs.jpcc.8b10200.
- (43) Yang, J.; Kim, M.; Lee, S.; Yoon, J. W.; Shome, S.; Bertens, K.; Song, H.; Lim, S. G.; Oh, J. T.; Bae, S. Y.; et al. Solvent Engineering of Colloidal Quantum Dot Inks for Scalable Fabrication of Photovoltaics. *ACS Appl Mater Interfaces* **2021**, *13* (31), 36992-37003. DOI: 10.1021/acsmi.1c06352 From NLM PubMed-not-MEDLINE.
- (44) Hamill, J. C.; Schwartz, J.; Loo, Y.-L. Influence of Solvent Coordination on Hybrid Organic–Inorganic Perovskite Formation. *ACS Energy Letters* **2017**, *3* (1), 92-97. DOI: 10.1021/acseenergylett.7b01057.
- (45) Akkerman QA, N. T., Boehme SC, Montanarella F, Dirin DN, Wechsler P, Beiglböck F, Rainò G, Erni R, Katan C, Even J, Kovalenko MV. . Controlling the nucleation and growth kinetics of lead halide perovskite quantum dots. *Science* **2022 Sep 23**;377(6613):1406-1412. doi: 10.1126/science.abq3616. Epub **2022 Sep 8**. PMID: 36074820.
- (46) Grisorio, R.; Quarta, D.; Fiore, A.; Carbone, L.; Suranna, G. P.; Giansante, C. The dynamic surface chemistry of colloidal metal chalcogenide quantum dots. *Nanoscale Advances* **2019**, *1* (9), 3639-3646, 10.1039/C9NA00452A. DOI: 10.1039/C9NA00452A.
- (47) U.V. Mardolcar, C. A. N. d. C., F.J.V. Santos. Dielectric Constant Measurements of Toluene and Benzene. *Fluid Phase Equilibria* **1992**.
- (48) Tironi, I. G.; Van Gunsteren, W. F. A molecular dynamics simulation study of chloroform. *Molecular Physics* **1994**, *83* (2), 381-403. DOI: 10.1080/00268979400101331.
- (49) Qiu, J.; Xue, W.; Wang, W.; Li, Y. Effective surface passivation on CsPbBr₃ nanocrystals via post-treatment with aromatic carboxylic acid. *Dyes and Pigments* **2022**, *198*. DOI: 10.1016/j.dyepig.2021.109806.
- (50) Zhang, X.; Bai, X.; Wu, H.; Zhang, X.; Sun, C.; Zhang, Y.; Zhang, W.; Zheng, W.; Yu, W. W.; Rogach, A. L. Water-Assisted Size and Shape Control of CsPbBr₃ Perovskite Nanocrystals. *Angew Chem Int Ed Engl* **2018**, *57* (13), 3337-3342. DOI: 10.1002/anie.201710869 From NLM PubMed-not-MEDLINE.
- (51) Peng, C.; Zhang, R.; Chen, H.; Liu, Y.; Zhang, S.; Fang, T.; Guo, R.; Zhang, J.; Shan, Q.; Jin, Y.; et al. A Demulsification–Crystallization Model for High-Quality Perovskite Nanocrystals. *Advanced Materials* **2023**, *35* (2), 2206969. DOI: <https://doi.org/10.1002/adma.202206969>.